Chemical Engineering Journal 485 (2024) 150011

Contents lists available at ScienceDirect

Chemical Engineering Journal

journal homepage: www.elsevier.com/locate/cej

Unlocking catalytic potential: Harnessing the power of oxidized active carbons for the hydrogenation of 1-chloro-4-nitrobenzene

Edgar S. Duran-Uribe, Antonio Sepúlveda-Escribano, Enrique V. Ramos-Fernandez *

Universidad de Alicante, Departamento de Química Inorgánica – Instituto Universitario de Materiales de Alicante (IUMA), Apartado 99, Alicante 03080, Spain

ARTICLE INFO

Keywords:
Oxidized activated carbon catalysts
Nitroarene hydrogenation
Surface functional groups

ABSTRACT

This study explores the effects of liquid-phase and gas-phase oxidation treatments on a low-ash activated carbon (RGC30) and its subsequent use as a metal-free catalyst for the hydrogenation of 1-chloro-4-nitrobenzene. Characterisation of the catalysts was accomplished through N_2 and CO_2 adsorption at −196 °C and 0 °C, respectively, together with techniques like X-ray photoelectron spectroscopy (XPS), Raman spectroscopy, thermogravimetric analysis (TGA) and temperature-programmed desorption (TPD). In particular, it is observed that the catalytic activity depends on the specific oxidation treatment applied, which leads to the generation of different oxygenated groups on the carbon surface. Consequently, through precise control of oxygen groups via thermal treatment under inert conditions, it is found that the most influential groups for the hydrogenation of 1-chloro-4-nitrobenzene are basic groups incorporating C═O bonds, such as quinones and carbonyls. Furthermore, certain groups, like phenols, exhibit a detrimental impact on the catalytic activity.

1. Introduction

In the realm of the chemical industry, substituted anilines are indispensable intermediates, playing a vital role in the synthesis of dyes, pharmaceuticals, and an array of other essential chemicals [1–3]. Due to its technological and environmental feasibility, the preferred route for the synthesis of amines is the reduction of substituted nitroarenes by heterogeneous catalysis [2,4–6]. The catalytic reduction of nitroarenes is usually carried out using reducing agents, with dihydrogen and hydrogen donors as hydrazine being the most commonly used sources [2,4–6]. The choice of these reducing agents hinges upon factors such as the catalyst employed, the substrate under consideration, and the technical and safety prerequisites inherent to the reaction [2,6]. Notably, despite its nature as a toxic and potentially carcinogenic, hydrazine boasts distinct merits over dihydrogen, which requires high pressures and temperatures to carry out the reaction [2,4–7]. These advantages encompass facile and secure manipulation, convenient storage, operation under mild reaction conditions, accelerated reaction rate, and non-toxic by-products (N_2 and H^+) [7–9]. Great efforts have been dedicated to developing catalysts tailored for the hydrogenation of nitroarenes [2,4]. A big part of these studies are related to the use of noble metals catalysts, renowned for their remarkable activity, but with some challenges, such as high cost and poor selectivity [2,4–6]. Meanwhile, catalysts rooted in non-noble metals, including Co or Ni, have shown specific activity, which is often accompanied by a high instability of the active phase [2,4,5,9,10]. Therefore, the search for cost-effective, chemically stable, and environmentally benign catalysts, yet remarkably active, stands as a topic of exploration within the academia and industry community.

In hydrogenation reactions, carbons materials have been widely used as catalyst support [11]. This is due to the carbons' easy preparation and controllable physicochemical properties, which allow a large surface area for distributing active phases, and they are cost-effective compared to other commercial supports [5,11,12]. Nevertheless, its application as a metal-free catalyst is less frequent, potentially due to the uniform charge distribution within the carbonaceous network, which makes it inert [13,14]. The inherent inertness of active carbon can be readily tailored through surface modification with heteroatoms [8,14–16]. The heteroatom doping leads to a reconfiguration of charge distribution across the carbon structure, yielding a metal-like electronic structure that significantly enhances the interaction of carbon with H_2 and the nitro group [14,16]. Various heteroatoms, including N, O, B, S, and P, have been used to modify the surface chemistry of carbon materials [14,16,17]. Among these, nitrogen and phosphorus doping has garnered significant attention in catalytic nitroarene reduction, revealing activity and selectivity in facilitating the synthesis of anilines [18].

* Corresponding author.
E-mail address: enrique.ramos@ua.es (E.V. Ramos-Fernandez).

https://doi.org/10.1016/j.cej.2024.150011
Received 10 November 2023; Received in revised form 18 February 2024; Accepted 24 February 2024
Available online 28 February 2024

The effect of oxygen on the surface chemistry of carbon materials has been the subject of study since the end of the 19th century [11,13,17]. Therefore, it is an interesting heteroatom when preparing carbons for use as metal-free catalysts; however, its study as an active site in the reduction of nitroarenes is still being determined. The interaction of oxygen with carbon atoms is relatively complex compared to other heteroatoms [17,19,20]. Unlike its counterparts, oxygen can bond in various ways with carbon, giving rise to a wide range of surface oxygenated complexes, as illustrated in Graph 1 [13,17,20,21]. These functional groups can modify to different extent the surface electronics of carbon and its hydrophilicity and acid-base properties. Furthermore, depending on the group introduced, different acidic or basic properties can be conferred on the surface (Graph 1) [17,21]. Therefore, they can also have different effects on the catalytic activity of carbons [17].

The composition and nature of oxygenated groups on the carbon surface can be manipulated through oxidation techniques and subsequent heat treatments under an inert atmosphere [20–22]. The strategic regulation of oxygenation holds significant importance in influencing the catalytic properties and performance of materials [21]. This provides a potential avenue for boosting catalytic activity.

In the state of the art of the use of oxidised carbon materials, testing has been conducted on carbon nanotubes (CNTs) for the reduction of nitro compounds, where it has been observed that C═O can play an important role [23]. Nonetheless, the unique physicochemical attributes of CNTs distinguish them from active carbons [18]. Consequently, the implications of oxygen and associated groups on amorphous mesoporous carbons is an area of interest for the reduction of aromatic nitrocompounds.

In this study, we present an exploration into the utilisation of metal-free catalysts based on oxidised activated carbons for the hydrogenation of 1-chloro-4-nitrobenzene using hydrazine as an H^+ donor. To achieve this, two distinct oxidation methods were employed. The first approach involved the utilisation of hydrogen peroxide (H_2O_2) at room temperature, while the second method encompassed the oxidation of the base carbon with diluted oxygen at elevated temperatures. Through this investigative approach, we elucidated the influence of the oxidation method on catalytic activity. Furthermore, we subjected the most active catalyst to meticulous thermal treatments at varying temperatures under inert conditions, revealing the distinct roles of various oxygen groups on the catalyst's surface.

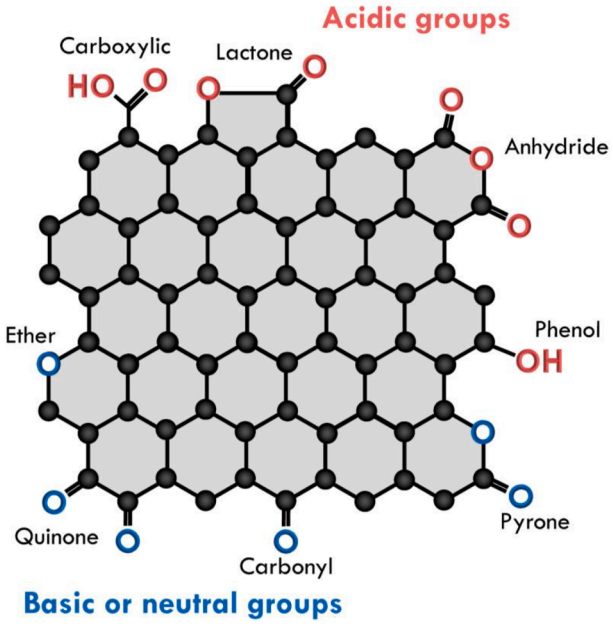

Graph 1. Oxygen-containing groups on activated carbon. . Adapted from [24]

2. Experimental section

2.1. Materials synthesis

A commercial low-ash activated carbon, RGC30, provided by West-Vaco Co., was subjected to two oxidation treatments. The first one was carried out in the liquid phase using a 6 M H_2O_2 solution. For this purpose, the RGC30 was dried in an oven at 60 °C for 12 h before treatment; then, the activated carbon was put in contact with the oxidising solution (50 ml/g_{RGC30}) for 48 h. Subsequently, the carbon was filtered and washed until the wash water had no oxidising character, which was determined using a potassium permanganate test (10^{-3} M HCl, 10^{-2} M $KMnO_4$). Finally, the carbon was dried overnight in an oven and stored in a desiccator. This catalyst was labelled ***ROX***.

The second treatment involved a thermal process conducted in an oxidising atmosphere, following the method outlined by Figuereido et al. [21]. The initial carbon sample was introduced into a U-shaped quartz reactor and then exposed to a thermal treatment at 450 °C for a duration of 10 h, utilising a 5 % O2 in He flows (50 ml·min^{-1}). Following the thermal treatment, the carbon material was placed within a desiccator to prevent moisture adsorption and was subsequently labelled as ***RO2_10H***.

Moreover, the *ROX* sample underwent diverse thermal treatments in an inert atmosphere. The procedure involved positioning the sample within an alumina crucible and subjecting it to varying temperatures (300, 500, 650, and 900 °C) using a tube furnace under a continuous N_2 flow (100 ml·min^{-1}). The heating rate was set at 3 °C·min^{-1}. The resulting samples were designated as ***ROX_Py***, where ***y*** corresponds to the temperature of the heat treatment.

2.2. Materials characterization

N_2 and CO_2 adsorption isotherms were measured at −196 °C and 0 °C, respectively, using a Quantachrome Instrument AUTOSORB-iQ-XR-2. Samples were out-gassed prior to adsorption measurements at 250 °C for 4 h under vacuum, using a Quantachrome Instrument Autosorb Degasser. Raman spectroscopy measurements were carried out on a Jasco NRS-5100 Raman system using a 633 nm laser and a 600 lines per mm slit. X-ray photoelectron spectroscopy (XPS) was performed with a K-Alpha spectrometer (Thermo Scientific). All spectra were collected using Mg-Kα radiation monochromatised by a double crystal monochromator with a hemispherical analyser. The binding energy for the XPS measurements was calibrated using the 1 s transition of C in the C-C bond (284.60 eV). Temperature-programmed desorption (TPD) experiments were carried out using a U-shaped reactor and 50 ml·min^{-1} of He. The released gases were measured with a mass spectrometer (Omnistar GSD 301 O2, Pfeiffer Vacuum). Thermogravimetric analysis (TGA) was performed using a TGA/STA 449 F5 Jupiter from NETZSCH. The TGA measurement was obtained from room temperature to 1000 °C using a heating ramp of 10 °C·min^{-1} under an inert atmosphere.

2.3. Catalytic test

After the oxidation treatment, the catalysts were tested for the hydrogenation of 1-chloro-4-ntitrobenzene (1C-4NB). The catalytic experiments were conducted at atmospheric pressure in a 100 ml three-neck round-bottom flask equipped with an aliquot system. The experiments were performed under the following conditions: 50 ml of a 50 mM solution of 1-chloro-4-nitrobenzene in ethanol and 100 mg of catalyst at 80 °C and 300 rpm. In addition, 22 mmol of hydrazine (35 % wt. in H_2O) was used as a reducing agent. The liquid samples were analysed with a gas chromatograph equipped with a mass spectrometer and an HP-5 capillary column, using He as carrier gas. The recycling test was performed under the same conditions as described above. For this purpose,

the catalyst was recovered after the reaction by filtration and washing in ethanol, which was dried in an oven at 60 °C overnight.

3. Results

Fig. 1a. Shows the N_2 adsorption–desorption isotherms obtained for all the carbons. Table 1 summarises the main textural properties of the carbons before and after the oxidation treatments, obtained from N_2 (-196 °C) and CO_2 (0 °C) adsorption isotherms data. The starting carbon material, RGC30, displays a combination of type I and type IV(a) isotherms, as outlined in the IUPAC classification [25]. At low relative pressures, there is a large adsorption capacity related to micropore filling [25]. In the relative pressure range between 0 and 0.2, there is a large bend, indicating a very wide micropore size distribution [25]. As the relative pressure increases (>0.2), mesopore filling occurs [25]. Different paths in the adsorption and desorption brands (hysteresis cycle) are indicative of the presence of mesoporosity [25]. By scrutinising the textural parameters detailed in Table 1, it becomes evident that RGC30 is a micro-mesoporous carbon, with mesoporosity accounting for 54 % of its total porosity. As such, it can be considered as a suitable foundational material for our intended research, as the microporosity provides a high specific surface area, and the mesoporosity helps to avoid diffusional problems, which is very important, especially in liquid-phase reactions such as the one studied here.

The isotherms of the treated (oxidised) materials exhibit the same shape as those of the pristine material (RGC30). The only discernible difference lies in a slight reduction in the volume of microporosity. This phenomenon is attributed to blocking a fraction of micropores by the functional groups generated during the oxidation process, a phenomenon extensively explored in previous studies [25,26]. Furthermore, the textural parameters in Table 1 suggest a slight loss in specific surface area.

Fig. 1b shows the CO_2 isotherms at 0 °C of the investigated carbon materials. Observably, the CO_2 adsorption capacity of the ROX sample is slightly less than that of RO2_10H. This disparity is further highlighted in Table 1, illustrating that the ROX sample's micropore volume is marginally smaller than that of the RO2_10H sample. However, this slight difference is not considered significant. Moreover, when comparing the micropore volumes obtained from N_2 adsorption with those obtained from CO_2 adsorption, it can be seen that Vmicro N_2 > Vmicro CO_2, what corroborates the wide micropore size distribution of these materials.

The oxidised carbons have similar adsorption capacities (N_2 and CO_2) and textural parameters. Therefore, the oxidation treatment does not significantly affect the porous structure of the carbon.

Table 1
Textural properties of activated carbon before and after oxidation treatment.

Sample	S_{BET} /$m^2 \cdot g^{-1}$	V_{total} /$cc \cdot g^{-1}$	$V_{micro}N_2$ /$cc \cdot g^{-1}$	$V_{micro}CO_2$ /$cc \cdot g^{-1}$	V_{meso} /$cc \cdot g^{-1}$
RGC30	1518	1.14	0.52	0.34	0.62
RO2_10H	1403	1.16	0.46	0.34	0.70
ROX	1405	1.13	0.51	0.29	0.62

Raman profiles for the samples before and after the oxidation treatments are displayed in Fig. 2a. Generally, no relevant changes were observed with the type of oxidation treatment. The typical D (1338 cm^{-1}) and G (1598 cm^{-1}) bands, characteristics of activated carbon, were shown by all the samples. The D peak is related to the disordered carbon, whereas the G band can be ascribed to the graphitic structure of the material [27]. To measure the degree of order/disorder of the investigated carbons, the ratio of D-band and G-band intensities (I_D/I_G) was calculated (Fig. 2a). A slight increase in the calculated I_D/I_G value was observed for oxidised carbons, indicating that the oxidation treatment slightly increased the disorder in the turbostratic structure [27]. However, the observed effect is weak.

XPS measurements were performed to gain insight into the oxygen functional groups on the surfaces of the investigated carbons. Fig. 2s shows the XPS survey of the oxidised samples and the RGC-30. In all cases two peaks were observed, the first one an intense peak over 285 eV related to the C1s transition of the carbon. Subsequently a smaller peak over 533 eV related to the O1s transition of oxygen. This indicates that the carbon samples consist primarily of carbon, oxygen, and hydrogen. For a more detailed analysis of the chemical environment of carbon and oxygen, high-resolution XPS measurements were conducted, as depicted in Fig. 2b. The deconvoluted C1s core level spectra for the investigated materials (Fig. 2b) exhibit four distinct contributions. The first and most intense peak (peak I) is observed at ~284.6 eV and corresponds to the C-C sp^2 bond [20,28]. The second peak (peak II) appears in the 285.8–286.0 eV range and is attributed to the C-O bond of phenolic, alcohol, or ether groups [20,28]. The third peak (peak III), observed between 286.9 and 287.9 eV, is related to the C═O bond of carbonyl or quinone groups [20,28]. Finally, a fourth peak (peak IV) is observed at a higher binding energy, between 288.2 and –289.9 eV, and is associated with the COO bond of carboxylic acids (CA) [20,28].

On the other hand, three contributions can be observed upon analysing the O1s core level spectra of the investigated carbons. Firstly, a contribution at around 531.1 – 531.4 eV (peak I) is attributed to the oxygen in the carbonyl and quinone groups [20,28]. Secondly, an intense peak over 532.7–533.0 eV, which is characteristic of the oxygen contained in ether, ester, and anhydride groups [20,28]. Finally, a peak

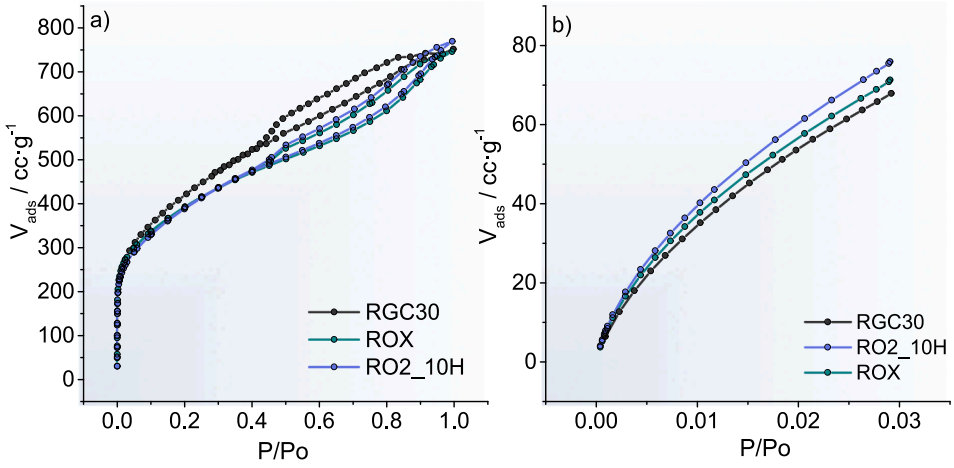

Fig. 1. A) N_2 adsorption isotherms at −196 °C for the pristine carbon and the samples treated with H_2O_2 and O_2. **b)** CO_2 adsorption isotherms at 0 °C for the pristine carbon and for the samples treated with H_2O_2 and O_2.

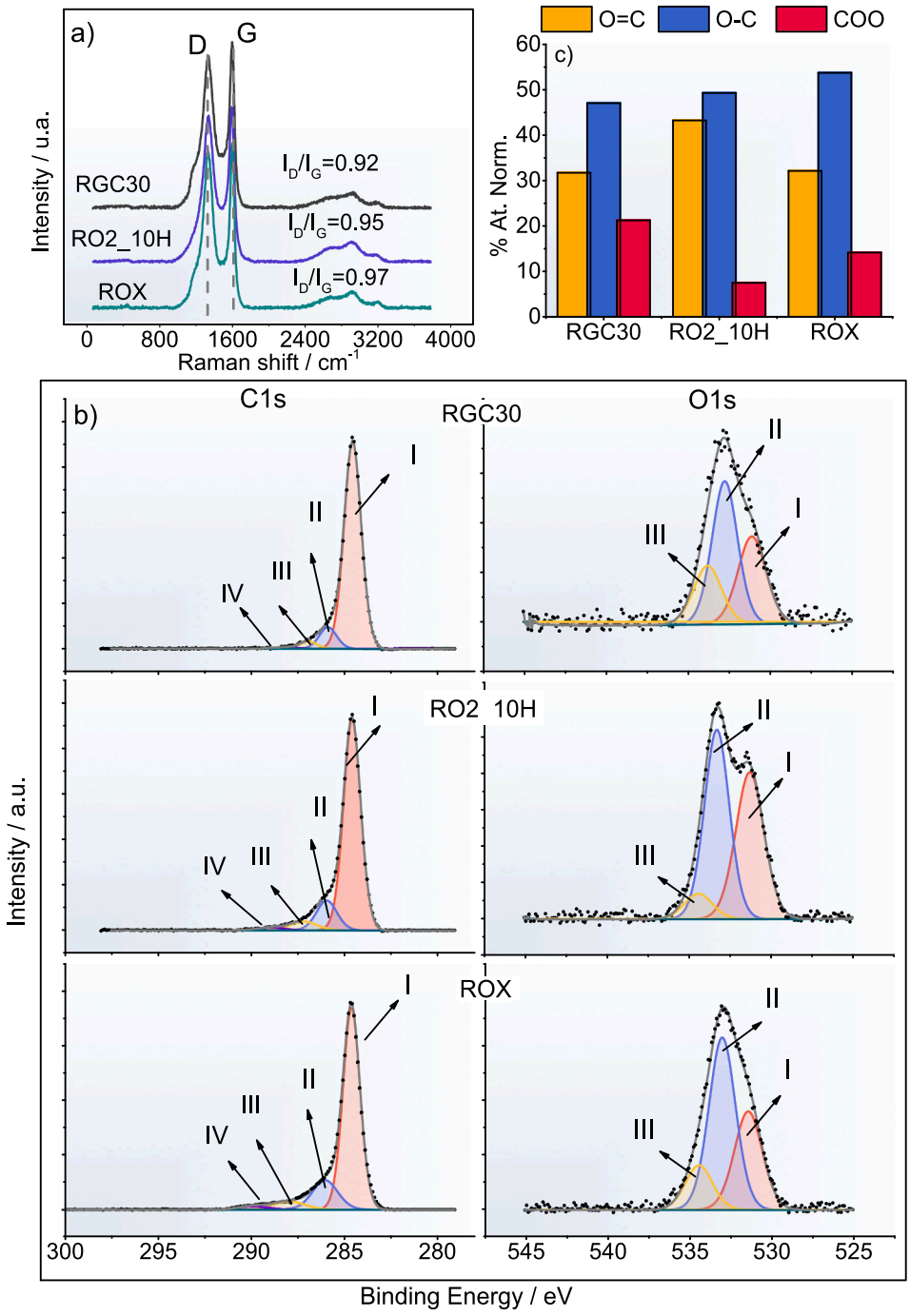

Fig. 2. A) Raman profile for RGC30, ROX and RO2_10H. **b)** High-resolution XPS spectra of RGC30, ROX and RO2_10H. **c)** Normalised O1s core level from XPS data for carbons before and after the oxidation treatments.

(III) within 533.8–534.4 eV can be observed, related to the oxygen in carboxylic acids [20,28].

Tables 2 and 3 summarise the variation in atomic percentage for the different species obtained from the deconvoluted O1s and C1s core level spectra, respectively. The primary observation is an increase in the O/C fraction in the oxidised samples, signifying the efficacy of the oxidation treatments. Notably, the method that demonstrated the highest success in incorporating oxygen into the carbon matrix was the use of diluted oxygen at 450 °C (RO2_10H), as evidenced by an XPS O/C ratio of 0.12. In contrast, oxidation with H2O2 yielded an XPS O/C ratio of 0.088. Hence, the total oxygen content of the samples follows the order of RO2_10H > ROX > RGC30.

Table 2
XPS results for the O1s core level spectra for the samples before and after the oxidation treatment. * The O/C ratio was calculated using the total content of O1s and C1s provided by XPS data.

Sample	O1s			O/C*
	Peak I O=C % At. Rel.	Peak II O-C % At. Rel.	Peak III COO % At. Rel.	
RGC30	1.18	1.75	0.79	0.039
RO2_10H	4.51	5.14	0.78	0.12
ROX	2.59	4.33	1.14	0.088

Table 3
XPS results for the C1s core level spectra for the samples before and after the oxidation treatment.

Sample	C1s			
	Peak I C-C %At. Rel.	Peak II C-O/C-OH %At. Rel.	Peak III C═O %At. Rel.	Peak IV COO %At. Rel.
RGC30	83.62	8.77	2.96	0.92
RO2_10H	71.25	12.04	4.72	1.56
ROX	69.27	15.03	5.47	2.16

Table 2 illustrates the influence of the oxidation method on the oxygen speciation within the carbon structure. Notably, carbon RO2_10H displayed the highest presence of carbonyl and quinone-related groups (Peak I). On the other hand, carbon ROX exhibited a more substantial contribution of carboxylic acid groups (Peak III), with no significant increase compared to RGC30 observed in sample RO2_10H. Additionally, both methods led to a comparable increase in O-C groups.

Table 3 shows a noticeable decrease in graphitic carbon bonds (Peak I) after the oxidation treatment, whereas the peaks related to oxygen-bonded carbon increase in intensity, as could be expected from the increase of the surface oxygen content upon the oxidation treatments.

Upon normalising the content of each contribution in the O1s region to the total surface oxygen determined by XPS (Fig. 2c), discernible variations in oxygen speciation become apparent, contingent upon the oxidation method. The distribution obtained for the pristine and the treated carbons was O-C > O = C > COO. Both oxidation methods increase the content of O-C and O═C groups more than that of COO groups. Among the samples, RO2_10H has the lowest COO content, which can be attributed to the instability of these groups at the temperature at which the oxidation treatment was carried out, 450 °C [20,21]. Moreover, oxidation with oxygen favors the formation of O═C groups, while treatment with H_2O_2 leads to an increase in the number of C-O groups. This observation stems from the synthesis of the RO2_10H sample. In the oxidation treatment at 450 °C, reactive carbon sites develop due to the decomposition of acidic groups in the pristine carbon (RGC30), as these groups become unstable at this temperature. Subsequently, these reactive carbon sites react with oxygen molecules in the stream, forming carbonyl species [13,17]. Moreover, a comparable phenomenon will occur during storage; if any carbon sites are available after treatment, they react with oxygen molecules in the air [17].

To better understand the content of oxygen in the bulk material, thermogravimetric analysis (TGA) was conducted under an inert atmosphere, as oxygenated groups will thermally decompose at different temperatures. Fig. 3 shows the TGA profiles and their corresponding derivative (DTG) of the studied samples, where it can be observed that, depending on the oxidation treatment, different mass loss profiles with respect to the pristine sample can be obtained. Thus, the pristine sample (RGC30) shows a slight mass loss, especially at high temperatures, showing the main mass loss at 922 °C. On the other hand, at low temperatures, the RO2_10H sample has a thermogram to that of RGC30 until point I at 460 °C; subsequently, a sharp increase in the mass loss until 1000 °C is observed. In this range, the RO2_10H presents a main mass loss at 700 °C, and later, a small shoulder at 922 °C can be observed on the DTG. Otherwise, the ROX sample shows a gradual mass loss from 100 °C to 1000 °C; upon observing the DTG, peaks at 180, 700 and 922 °C are observed. When comparing the mass losses between the samples, it is observed that RO2_10H is the sample that lost the most mass during the analysis, followed by ROX and finally RGC30 (Fig. 3). This agrees with what was observed by XPS, where the gas phase oxidised sample (RO2_10H) showed the highest oxygen content on its surface. Nonetheless, these findings also shed light on the group diversity in the samples. The ROX sample emerges as the most chemically diverse, highlighted by the distinct peaks observed in the TGA results, closely associated with various oxygen groups [20,21,29]. In contrast, the thermogravimetric profile of the RO2_10H sample implies that it represents a carbon with a less diverse range of groups despite having a higher oxygen content. However, the TGA results strongly indicate the oxygen inclusion in the carbon and the oxygen diversity at the carbon surface for each oxidation method. Temperature-programmed desorption (TPD) experiments were conducted under identical conditions to gain insights into the nature of the surface chemistry O-containing groups in the carbons (Fig. 4). It is crucial to emphasise that the TPD experiments involved monitoring various masses, including CO, CO_2, H_2O, and CH_4 The absence of gases related to H_2O or CH_4 (Fig. 1s) emissions from the sample was notable, affirming a direct correlation between the observed mass loss in TGA and the thermal decomposition processes of oxygenated groups.

Fig. 4a shows the CO_2 evolution profiles in temperature-programmed desorption (TPD) experiments for the investigated carbons. The CO_2 (44 *m/z*) released from the RGC30 sample shows a low content of acid groups, with two broad and small peaks; the first one is associated with the decomposition of carboxylic acids (CA, decomposition temperature: 100–450 °C) and the second one with the decomposition of lactones (LC, decomposition temperature: 600–800 °C) [20,29]. As was shown in TGA experiments (Fig. 6), the RO2_10H sample does not lose mass until 480 °C. This outcome is anticipated due to the instability of carboxylic acid (CA) groups at 450 °C [20,21,29]. Furthermore, this temperature promotes the decomposition of CA groups from the pristine sample [20,22]. However, an abrupt increase in the release of μmol of CO_2 can be observed at temperatures above 400 °C, which is related to the decomposition of acid groups as LC and basic groups as pyrone (Py decomposition temperature >900 °C) [20,21,29]. On the other hand, the CO_2 profile observed in the ROX sample can be linked to the

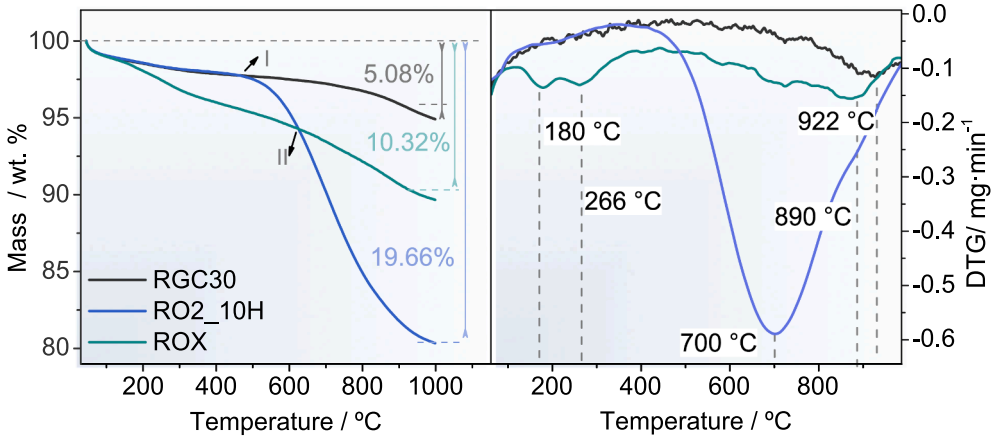

Fig. 3. TGA and DTG profile under an inert atmosphere for the pristine and oxidised samples.

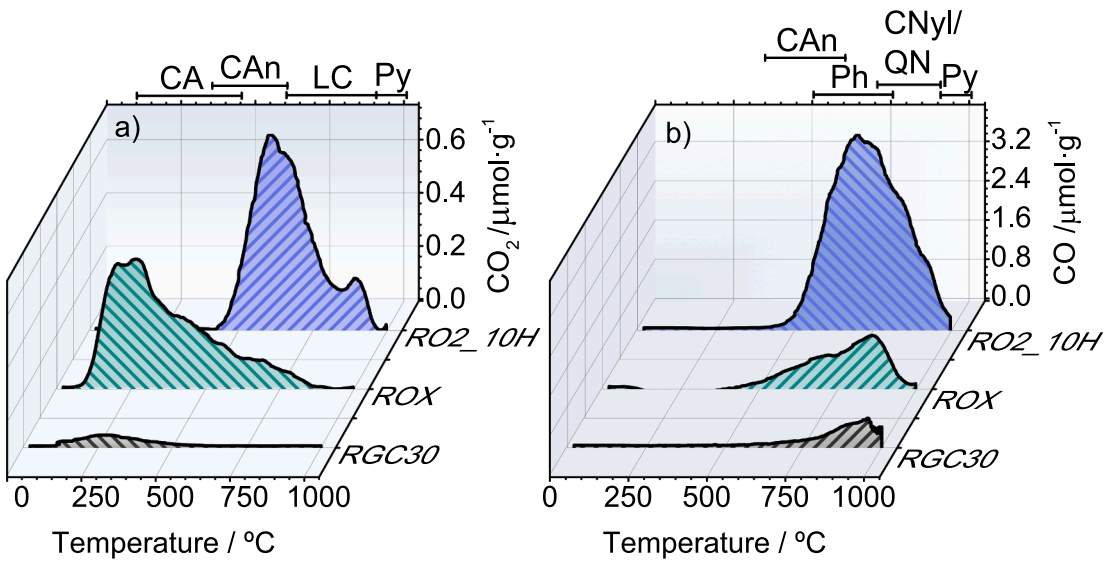

Fig. 4. TPD Profiles of CO_2 **(a.)** and CO **(b.)** from RGC30, ROX and RO2_10H. Carboxylic acid (CA), carboxylic anhydride (CAn), Lactone (LC), phenol (Ph), carbonyl (CNyl), quinone (QN), Pyrone (Py).

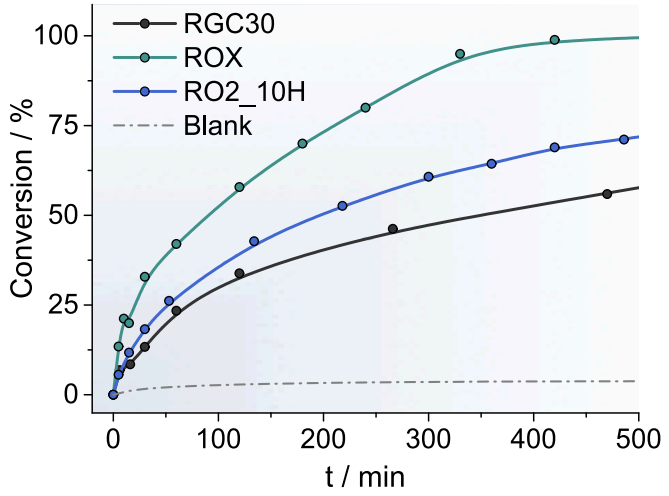

Fig. 5. Catalytic test for oxidised and pristine carbon for the hydrogenation of 1-chloro-4-nitrobence. (m_{cat} = 100 mg, $n_{susbtrate}$ = 2.52 mmol, $n_{hydrazine}$ = 1.85 mmol, T = 80 °C, $V_{solution}$ = 50 ml).

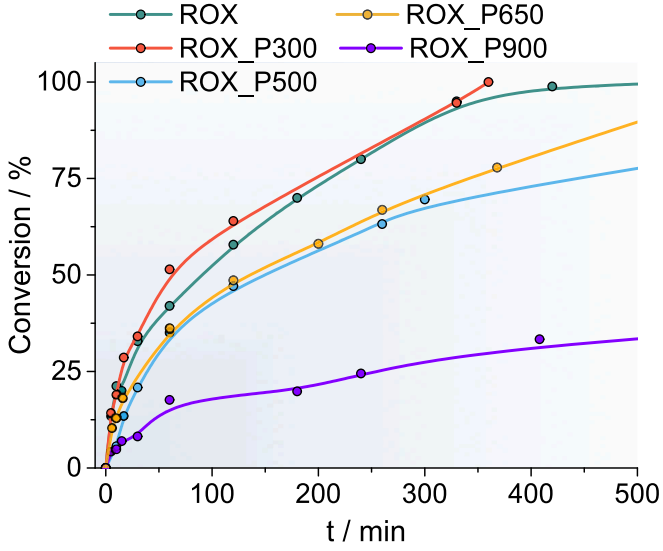

Fig. 6. Catalytic test of ROX treated at different temperatures under N_2 atmosphere. (m_{cat} = 100 mg, $n_{susbtrate}$ = 2.52 mmol, $n_{hydrazine}$ = 1.85 mmol, T = 80 °C, $V_{solution}$ = 50 ml).

decomposition of carboxylic acid (CA) groups at lower temperatures (100–450 °C), resulting in a relatively higher mass loss for the ROX sample compared to the other samples (Fig. 3). In addition, there is a second peak (600–800 °C) associated to LC when the temperature of the experiment increases. Nevertheless, the signal indicating CO_2 evolution within this temperature range is more prominent for the RO2_10H sample than the ROX sample. This can be attributed to a higher concentration of lactones and pyrone groups on the carbon surface in the RO2_10H sample.

The CO (28 *m/z*) evolution profile in TPD experiments is shown in Fig. 4b. The profile corresponding to the RGC30 sample shows a broad peak near 900 °C, related to the decomposition of carbonyl/quinone groups (CNyl/QN, decomposition temperature: 700–950 °C) [20–22,29]. After the oxidation treatment, the RO2_10H sample shows a higher amount of CO released than ROX, which agrees with the mass loss observed in the TGA experiment. The profiles corresponding to samples RO2_10H and ROX show decomposition peaks assigned to phenol (Ph, decomposition temperature: 500–750 °C) and CNyl/ QN groups [20–22,29]. However, although the ROX sample has a lower content of these basic groups, it shows a preference for the inclusion of QNyl/QN groups (peak above 900 °C), compared to the RO2_10H sample, which shows a preference for Ph groups, since the CO signal maximum is found in these groups respectively for each sample.

These findings are consistent with the results from XPS analysis, where the ROX sample exhibited a higher content of carboxylate (COO) groups than RO2_10H. Thus, it is shown that the oxidation method affects the content and type of O functional groups in the catalysts, with RO2_10H being the richest in surface oxygen with the highest concentration of C═O and C-O groups. On the other hand, the ROX catalyst shows a significant increase in the COO group. However, the ROX catalyst also showed a tendency for CNyl and QN groups to be formed preferentially over other groups, such as Ph.

After characterising the physicochemical properties of the three activated carbons were evaluated in the selective hydrogenation of 1-chloro-4-nitrobence (1C-4NB) using hydrazine as a reducing agent. The results are presented in Fig. 5. Notably, no conversion of nitroarenes

was observed when the reaction was conducted without any catalyst. However, the oxidised samples exhibited higher catalytic activity than the untreated (RGC30). This suggests that the presence of oxygenated functional groups in the samples significantly influences their catalytic performance. Interestingly, the ROX sample demonstrated superior performance to RO2_10H despite showing less oxygen content on its surface. This indicates that the type of oxygenated groups in the material also plays a crucial role in catalytic activity, emphasising the importance of specific functional groups for enhanced performance.

Table 4 summarises the kinetic constant (k), yields and selectivity toward 4-chloroaniline (4-ChAn) for the investigated carbons at 420 min of reaction. The kinetic constant was calculated from the data obtained at low reaction times, assuming a first-order reaction. In all cases, the selectivity for 4-ChAn was over 100 %. Nevertheless, 4-ChAn yield and kinetic constant (k) change according to the oxidation treatment. Thus, the carbon treated with H_2O_2 (ROX) exhibits a higher yield (100 %) and k value (0.013) for the hydrogenation of 4-ChAn than the RO2_10H sample. To investigate the specific functional groups that contribute to the catalytic reaction, we focused on the most active sample, ROX, and conducted a series of experiments. Our goal was to discern the influence of various functional groups on catalytic activity. To achieve this, we exposed the active carbon to different temperatures under an inert atmosphere. This approach allowed us to selectively eliminate certain functional groups and assess their impact on catalytic performance [20,21]. By observing the changes in activity as different functional groups were removed, we aimed to identify the key contributors to the catalytic reaction. Therefore, the ROX sample was treated at 300, 500, 650 and 900 °C under an inert atmosphere.

A thorough characterisation was performed before utilising these heat-treated samples as catalysts. Fig. 3s shows the N_2 adsorption isotherms for the treated samples. The treated samples have an adsorption–desorption profile like that of the ROX sample, associated with a micro-mesoporous material. Although, the ROX_P900 sample shows the main change, with a decrease in the adsorption capacity, related to a diminution in the microporosity. This effect can be observed in the CO_2 isotherms at 0 °C (Fig. 4s), where only the sample ROX_P900 shows a significant decrease in the adsorption capacity.

The analysis of the textural parameters (Table 1s) shows that the after the heat treatment there is a slight decrease in the specific surface, total pore volume and micropore volume, the sample with a significant decrease of the parameter values being the ROX_P900. Nevertheless, the mesopore volume does not show a significant variation in the samples, which is very important in liquid face reactions. Thus, the decomposition of the oxygenated groups affects mainly the microporosity of the carbon.

Raman studies (Fig. 5s) show no significant variation in the D (1338 cm^{-1}) and G (1598 cm^{-1}) bands of the heat-treated carbons, with the calculated index I_D/I_G oscillating in values close to those of the ROX sample (0.97), related to a semi-ordered carbon. Therefore, the microstructure is not significantly affected by thermal decomposition of oxygenated groups. Given the carbon's unaltered surface area and microstructure, any variations in catalytic activity can be attributed exclusively to the presence of oxygenated groups on the surface.

The catalytic assessment of the heat-treated ROX samples illustrates a discernible link between temperature and the extent of 1C-4NB conversion (Fig. 6). Notably, the sample treated at 300 °C maintains unaltered activity compared to the untreated sample. Conversely, an increase in the treatment temperature reduces catalytic conversion. Therefore, the samples treated at 500 and 650 °C (ROX_P500 and ROX_P650) exhibit decreased conversion, while ROX_P900 displays an even lower degree of conversion.

These outcomes align with expectations, as the source of catalytic activity lies within the surface oxygenated groups, which are compromised by the thermal treatments. Nonetheless, as we delve into the article's discussion, we will elucidate that the decrease in catalytic activity does not exhibit a linear relationship with temperature. The influence of losing certain surface functional groups outweighs that of others. Notably, even when the sample is treated at 300 °C, there is no catalytic activity change despite removing surface oxygen groups (See Table 5).

The XPS surveys of the inert-treated samples only show contributions related to C and O, such as the ROX sample. The high-resolution XPS spectra of the heat-treated samples are shown in Fig. 7. The C1s region shows that all the treated samples exhibit four contributions, similar to the ROX sample. Therefore, these contributions are related to C-C sp^2 bond (Peak I), C-O bond (Peak II), C═O bond (peak III) and COO bond (peak IV) [20,28]. From the C1s core level analysis, there is no significant reaction; there is a decrease in the COO bond contribution signal and an increase in the C-C sp^2 signal as the temperature increases (Table 6). This is related to the aforementioned loss of oxygen groups on the surface.

On the other hand, the O 1s core level spectra analysis for the heat-treated carbons showed significant changes in the carbon surface groups (Fig. 7, Table 7). Firstly, the XPS O/C ratio changes as the temperature increases up to 900 °C. Initially, for the ROX_P300 sample, it does not change significantly regarding the ROX sample. But it then decreases when the temperature increases until a value of 0.015 in the ROX_P900 sample. This is due to the decomposition of the oxygen groups during the thermal treatment [20,21,29]. On the other hand, initially, three contributions can be distinguished: O═C (peak I), O-C (peak II) and COO (peak III).

Regarding the oxygenated groups, there is a significant loss of COO species from the ROX_P300 sample. This is due to the instability of the carboxylic acid groups at temperatures higher than 100 °C [20,21,29]. Considering the other species (C-O and C═O), there is a gradual decomposition of the same degree for most of the carbons.

The distribution of surface oxygen species can be obtained from the XPS data by the normalisation of the O 1s region with the total O content (Fig. 8). It can be seen that there is a severe decrease in COO groups from the untreated ROX to ROX_P500. Though there is an enrichment in O═C bonds related to quinones and carbonyl groups, this occurs in the samples from P300 to P650, with the sample treated at 300 °C being the most affected by this trend. However, as the treatment temperature increases, the surface content of C═O bonds decreases. This can be related, on the one hand, to the fact that as the decomposition of oxygenated groups takes place, vacancies are generated that rearrange the surface carbon atoms [13,17]. In addition, the O═C amount tends to decrease until 650 °C, while the density of C-O bonds increases. Finally, the amount of C-O and C═O species decreases significantly after the treatment at 900 °C. However, there is a larger content of C═O than of C-O (Table 7, Fig. 8).

Fig. 9 presents the CO_2 and CO evolution profiles for the ROX and

Table 4
Kinetic constants and yield for 4-chloroaniline for the pristine and treated samples after 420 min. of reaction.

Catalyst	k / $s^{-1}{\cdot}g_{cat}^{-1}$	4-chloroaniline Yield / %	4-chloroaniline selectivity / %
RGC30	0.0044	55.91	100
RO2_10H	0.0055	68.91	100
ROX	0.013	100	100

Table 5
Kinetic constants, yield and selectivity for 4-chloroaniline for the ROX catalyst treated at different temperatures.

Catalyst	k / $s^{-1}{\cdot}g_{cat}^{-1}$	4-chloroaniline Yield / %	Selectivity/ %
ROX	0.013	100	100
ROX_P300	0.016	100	100
ROX_P500	0.0071	74.50	100
ROX_P650	0.0062	77.85	100
ROX_P900	0.0028	33.36	100

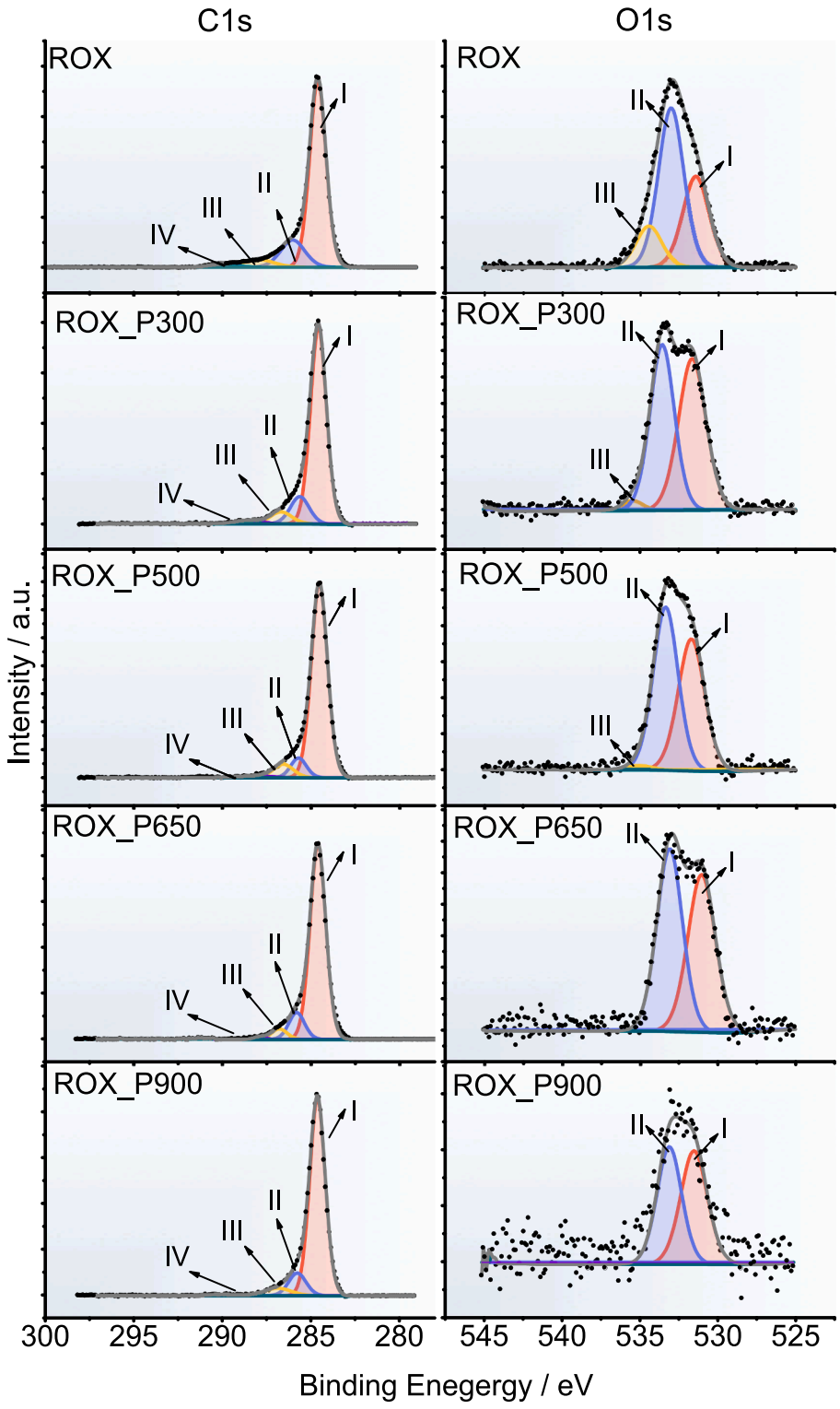

Fig. 7. High-resolution XPS spectra of ROX sample treated at different temperatures under an inert atmosphere.

thermally treated ROX samples in TPD experiments. The CO_2 profile (Fig. 9a) indicates an initial removal of carboxylic acid groups upon treatment at 300 °C. Additionally, carboxylic anhydride and lactones desorption are observed with increasing the treatment temperature, leading to a significant decay in the CO_2 signal for the ROX_P900 sample.

On the other hand, the CO signal profiles (Fig. 9b) show that the ROX_300 sample displays a shoulder peak above 450 °C, suggesting the presence of carboxylic anhydrides. Additionally, phenols and a prominent peak associated with carbonyls and quinones are observed for all the samples. As the temperature increases, the shoulder related to anhydrides and lactone diminishes, eventually disappearing until the treatment at P650 °C. At 650 °C, the primary functional groups in the catalyst are phenols and carbonyl/quinone species, with higher signal intensity compared to the P500 sample. The XCPS analysis corroborates this enrichment in phenols and quinones/carboxylic groups, indicating a

Table 6
XPS results for the C1s core level spectra for the ROX sample treated at different temperatures.

Sample	C1s			
	Peak I C-C %At. Rel.	Peak II C-O/C-OH %At. Rel.	Peak III C═O %At. Rel.	Peak IV COO %At. Rel.
ROX	69.27	15.03	5.47	2.16
ROX_P300	71.98	11.85	5.95	2.06
ROX_P500	77.31	7.61	6.7	1.49
ROX_P650	79.86	10.07	5.81	0.72
ROX_P900	81.72	10.59	5.45	0.79

Table 7
XPS results for the O1s core level spectra for ROX samples treated at different temperatures. * The O/C ratio was calculated using the total content of O1s and C1s provided by XPS data.

Sample	O1s			O/C*
	Peak I O═C % At. Rel.	Peak II O-C % At. Rel.	Peak III COO % At. Rel.	
ROX	2.59	4.33	1.14	0.088
ROX_P300	4.04	3.92	0.2	0.088
ROX_P500	3.13	3.65	0.1	0.074
ROX_P650	1.43	2.11	0.0	0.037
ROX_P900	0.74	0.7	0.0	0.015

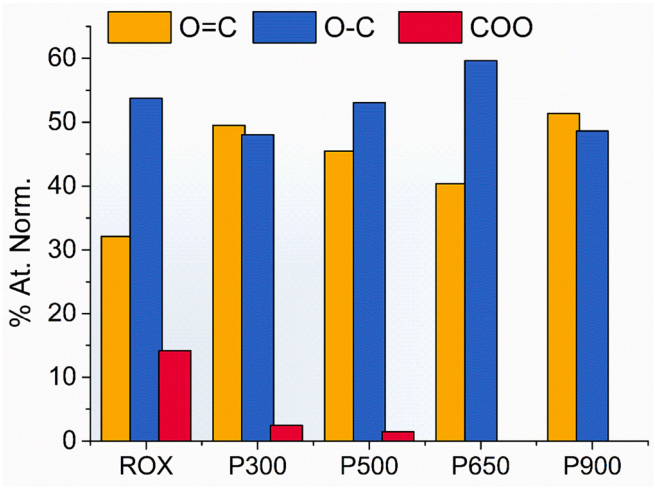

Fig. 8. Normalised amount of the different oxygenated species from the XPS O1s core level spectra for ROX carbons thermally treated at different temperatures.

d carbon rearrangement by the vances generated during desorption [13,20]. Furthermore, following the 900 °C treatment, a residual signal corresponding to a small amount of quinones and carbonyl groups persists. No pyrone group is detected, as the CO_2 signal is negligible at temperatures exceeding 900 °C.

4. Discussion

When the functional groups identified by XPS and TPD measurements correlate with the catalytic performance, the ROX sample reveals that carboxylic acid groups do not significantly impact the catalytic activity as active sites. This is evident as the loss of COO species does not result in diminished activity. Moreover, the closely matched activity of samples ROX_P500 and ROX_P600 suggests that the presence of lactone and anhydride groups does not play a pivotal role in the hydrogenation of 1-chloro-4-nitrobenzene. Rather, the remaining significant groups for samples ROX_P600 and P500 are phenol, carbonyl and quinone. Particularly noteworthy is the contribution of carbonyl and quinone groups, which have demonstrated their effectiveness as the active phase in the reduction of 1C-4NB using oxidised nanotubes in the presence of hydrazine as the reducing agent [23,30].

However, intriguingly, the P900 catalyst in this study shares a comparable C═O content with RGC30, yet it displays distinct catalytic activity despite the presence of carbonyl and quinone groups. This outcome underscores the significance of phenol, carbonyl, and quinone groups as essential active sites for nitroarene reduction. Yet, the comparison between the activity of the ROX sample and the RO2_10H sample unveils an intricate interplay of oxygen groups, especially basic groups like quinones and carbonyls. This leads us to the realisation that not only the oxygen content but also a judicious arrangement of functional groups is vital for the catalytic reaction.

Therefore, it appears that an optimal balance of functional groups is pivotal. A higher prevalence of carbonyl and quinone groups in relation to phenol content seems to yield more favourable results for the reaction. This phenomenon could stem from the excessive presence of phenolic groups potentially interfering negatively with the adsorption of the nitro group. This inference aligns with the tendency of the nitro group to engage more favourably with basic adsorption sites [31].

5. Recycling test

To assess the catalyst's stability, a reuse test was conducted on the ROX sample (Fig. 10a). It's worth noting that the selectivity towards CA remains unaltered across the different cycles. The catalytic assessments unveil a consistent and sustained sample activity even after five consecutive reaction cycles, accompanied by a slight elevation in catalyst conversion. To gain deeper insights into the catalyst's behaviour, post-cycling XPS measurements were conducted on the sample after the fifth cycle (ROX_C5).

The XPS analysis of the ROX sample after the fifth cycle (ROX_C5) reveals a similarity in the speciation of C═O, C-O, and COO bonds compared to the pristine sample, as illustrated in Fig. 7s and Fig. 10b. Examination of the XPS data further indicates a marginal shift in the O/C ratio, transitioning from 0.088 for the ROX sample to 0.11 for the ROX_C5 sample. This subtle alteration is thought to be due to the contact of the catalyst with oxygen in the air and is responsible for the increased conversion.

Notably, the absence of significant structural changes suggests that the sample maintains stability at the surface level. The preservation of oxygen groups and the retention of robust catalytic activity after each cycle affirm the resilience of the catalyst, emphasising its potential for enduring performance across multiple reaction cycles.

6. Conclusions

In this study, we developed oxidised activated carbon catalysts for the hydrogenation of 1-chloro-4-nitrobenzene, revealing the superior efficacy of the oxidation treatment with hydrogen peroxide compared to high-temperature oxygen exposure as the route for generating oxygen surface groups. Furthermore, the chosen treatment significantly influenced the distribution of surface functional groups, and it has been shown that phenol, carbonyl, and quinone groups emerge as pivotal to catalytic activity. Notably, the balance of these groups directly impacted activity; maintaining a lower phenol content in relation to quinone and carbonyl groups proved crucial for optimal catalytic performance. These results show the use of oxidised carbons as potential catalysts for the hydrogenation of halogenated nitroarenes. The study accentuates the significance of precise types and arrangements of oxygenated groups in achieving enhanced catalytic outcomes.

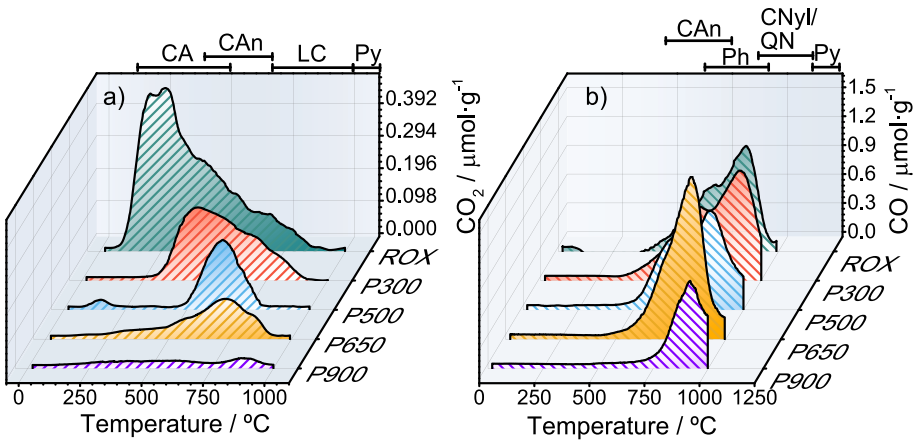

Fig. 9. TPD profiles of CO_2 (a) and CO (b) from ROX samples treated at different temperatures. Carboxylic acids (CA), carboxylic anhydride (CAn), lactone (LC), pyrone (Py), phenol (Ph), Carbonyl and quinone (CNyl/QN).

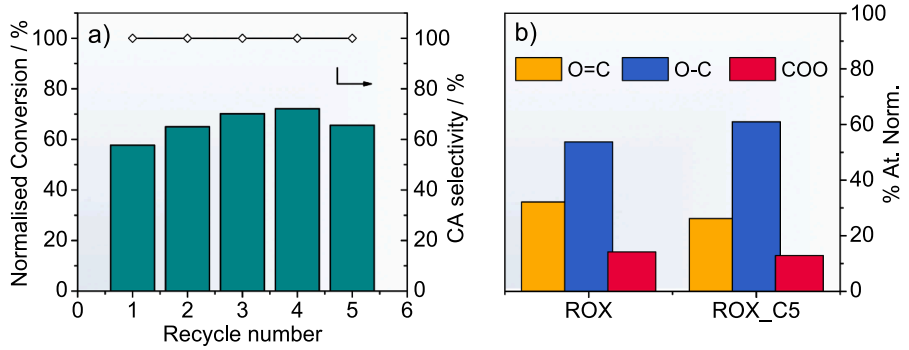

Fig. 10. ROX Catalyst recycling test. (m_{cat} = 100 mg, $n_{susbtrate}$ = 2.52 mmol, $n_{hydrazine}$ = 1.85 mmol, T = 80 °C, $V_{solution}$ = 50 ml, reaction time = 120 min).

CRediT authorship contribution statement

Edgar S. Duran-Uribe: . **Antonio Sepúlveda-Escribano:** Writing – review & editing, Supervision, Funding acquisition, Conceptualization. **Enrique V. Ramos-Fernandez:** Writing – review & editing, Writing – original draft, Funding acquisition, Formal analysis, Conceptualization.

Declaration of competing interest

The authors declare that they have no known competing financial interests or personal relationships that could have appeared to influence the work reported in this paper.

Data availability

No data was used for the research described in the article.

Acknowledgements

Financial support from Ministerio de Ciencia e Innovación (Spain, project PID1019-108453GB-C21 and PID2020-116998RB-I00) is gratefully acknowledged. ESDU also thanks Consellería de Innovación, Universidaddes Ciancia y Sociedad Digital (Generalitat Valenciana, Spain) for his GRISOLIAP/2020/123 grant and CIPROM/2021/022. This study forms part of the Advanced Materials programme and was supported by MCIN with funding from European Union NextGenerationEU (PRTR-C17.I1) and by Generalitat Valenciana.

References

[1] P.F. Vogt, J. Gerulis, Amines, aromatic, in: Ullmann's Encyclopedia of Industrial Chemistry, Wiley, 2000, https://doi.org/10.1002/14356007.a02_037.
[2] R. Gao, C. Peng, J. Zou, Selective catalytic hydrogenation of nitroarenes to anilines, in: Industrial Arene Chemistry, Wiley, 2023, pp. 1479–1524, https://doi.org/10.1002/9783527827992.ch50.
[3] M. Anjalin, N. Kanagathara, A.R. Baby Suganthi, A brief review on aniline and its derivatives, Mater. Today:. Proc. 33 (2020) 4751–4755, https://doi.org/10.1016/J.MATPR.2020.08.358.
[4] G. Liu, C. Chen, J. Chen, Catalytic and electrocatalytic hydrogenation of nitroarenes, J. Phys. Chem. C 127 (2023) 4375–4386, https://doi.org/10.1021/acs.jpcc.3c00270.
[5] J. Song, Z.F. Huang, L. Pan, K. Li, X. Zhang, L. Wang, J.J. Zou, Review on selective hydrogenation of nitroarene by catalytic, photocatalytic and electrocatalytic reactions, Appl. Catal. B 227 (2018) 386–408, https://doi.org/10.1016/j.apcatb.2018.01.052.
[6] G. Booth, Nitro compounds, aromatic, ullmann's encyclopedia of industrial, Chemistry (2000), https://doi.org/10.1002/14356007.A17_411.
[7] G. Lu, K. Sun, Y. Lin, Q. Du, J. Zhang, K. Wang, P. Wang, Single-atomic-site iron on N-doped carbon for chemoselective reduction of nitroarenes, Nano Res. 15 (2022) 603–611, https://doi.org/10.1007/s12274-021-3526-5.
[8] S. Abednatanzi, P. Gohari Derakhshandeh, S. Dalapati, S.K.P. Veerapandian, A.-C. Froissart, J.D. Epping, R. Morent, N. De Geyter, P. Van Der Voort, Metal-free chemoselective reduction of nitroarenes catalyzed by covalent triazine frameworks: the role of embedded heteroatoms, ACS Appl. Mater. Interfaces 14 (2022) 15287–15297, https://doi.org/10.1021/acsami.2c01091.
[9] Y. Duan, T. Song, X. Dong, Y. Yang, Enhanced catalytic performance of cobalt nanoparticles coated with a N, P-codoped carbon shell derived from biomass for transfer hydrogenation of functionalized nitroarenes, Green Chem. 20 (2018) 2821–2828, https://doi.org/10.1039/C8GC00619A.
[10] J.J. Villora-Picó, I. Campello-Gómez, J.C. Serrano-Ruiz, M.M. Pastor-Blas, A. Sepúlveda-Escribano, E.V. Ramos-Fernández, Catalysis Science & Technology Hydrogenation of 4-nitrochlorobenzene catalysed by cobalt nanoparticles supported on nitrogen-doped activated carbon, Cat. Sci. Technol. 11 (2021) 3845, https://doi.org/10.1039/d1cy00140j.
[11] F. Rodríguez-Reinoso, A. Sepúlveda-Escribano, Carbon as Catalyst Support, in: Carbon Materials for Catalysis, Wiley, 2008: pp. 131–155. https://doi.org/10.1002/9780470403709.ch4.

[12] H. Marsh, F. Rodríguez-Reinoso, Applicability of Activated Carbon, in: H. Marsh, F. Rodríguez-Reinoso (Eds.), Activated Carbon, Elsevier, Oxford, 2006: pp. 383–453. https://doi.org/10.1016/B978-008044463-5/50022-4.
[13] H. Marsh, F. Rodríguez-Reinoso, Activated Carbon (Origins), in: H. Marsh, F. Rodríguez-Reinoso (Eds.), Activated Carbon, Elsevier, Oxford, 2006: pp. 13–86. https://doi.org/10.1016/B978-008044463-5/50016-9.
[14] X. Liu, L. Dai, Carbon-based metal-free catalysts, Nat. Rev. Mater. 1 (2016) 16064, https://doi.org/10.1038/natrevmats.2016.64.
[15] C. Hu, L. Dai, Doping of carbon materials for metal-free electrocatalysis, Adv. Mater. 31 (2019) 1804672, https://doi.org/10.1002/adma.201804672.
[16] Y. Rangraz, M.M. Heravi, Recent advances in metal-free heteroatom-doped carbon heterogonous catalysts, RSC Adv. 11 (2021) 23725–23778, https://doi.org/10.1039/D1RA03446D.
[17] T.J. Bandosz, C.O. Ania, Chapter 4 Surface chemistry of activated carbons and its characterization, in: T.J. Bandosz (Ed.), Interface Science and Technology, Elsevier, 2006: pp. 159–229. https://doi.org/10.1016/S1573-4285(06)80013-X.
[18] J. Yao, L. Wang, D. Xie, L. Jiang, J. Li, X. Fang, Nanocarbon-based catalysts for selective nitroaromatic hydrogenation: a mini review, Front. Chem. 10 (2022), https://doi.org/10.3389/fchem.2022.1000680.
[19] Y. Gao, Q. Wang, G. Ji, A. Li, J. Niu, Doping strategy, properties and application of heteroatom-doped ordered mesoporous carbon, RSC Adv. 11 (2021) 5361–5383, https://doi.org/10.1039/D0RA08993A.
[20] R.P. Rocha, M.F.R. Pereira, J.L. Figueiredo, Characterisation of the surface chemistry of carbon materials by temperature-programmed desorption: an assessment, Catal. Today 418 (2023) 114136, https://doi.org/10.1016/j.cattod.2023.114136.
[21] J.L. Figueiredo, M.F.R. Pereira, M.M.A. Freitas, J.J.M. Órfão, Modification of the surface chemistry of activated carbons, Carbon N y. 37 (1999) 1379–1389, https://doi.org/10.1016/S0008-6223(98)00333-9.
[22] S. Barrientos-Ramírez, G. Montes de Oca-Ramírez, E.V. Ramos-Fernández, A. Sepúlveda-Escribano, M.M. Pastor-Blas, A. González-Montiel, F. Rodríguez-Reinoso, Influence of the surface chemistry of activated carbons on the ATRP catalysis of methyl methacrylate polymerization, Appl. Catal. A 397 (2011) 225–233, https://doi.org/10.1016/j.apcata.2011.03.004.
[23] S. Wu, G. Wen, R. Schlögl, D.S. Su, Carbon nanotubes oxidised by a green method as efficient metal-free catalysts for nitroarene reduction, PCCP 17 (2015) 1567–1571, https://doi.org/10.1039/C4CP04658G.
[24] M.N. Nagornaya, G.I. Razdyakonova, S.Y. Khodakova, The effect of functional groups of carbon black on rubber properties, Procedia Eng. 152 (2016) 563–569, https://doi.org/10.1016/j.proeng.2016.07.656.
[25] M. Thommes, K. Kaneko, A. V Neimark, J.P. Olivier, F. Rodriguez-Reinoso, J. Rouquerol, K.S.W. Sing, Physisorption of gases, with special reference to the evaluation of surface area and pore size distribution (IUPAC Technical Report), 87 (2015) 1051–1069. https://doi.org/doi:10.1515/pac-2014-1117.
[26] E.V. Ramos-Fernández, J.C. Serrano-Ruiz, J. Silvestre-Albero, A. Sepúlveda-Escribano, F. Rodríguez-Reinoso, The effect of the cerium precursor and the carbon surface chemistry on the dispersion of ceria on activated carbon, J. Mater. Sci. 43 (2008) 1525–1531, https://doi.org/10.1007/s10853-007-2361-8.
[27] Y. Kaburagi, A. Yoshida, Y. Hishiyama, Raman Spectroscopy, in M. Inagaki, F. Kang (Eds.), Materials Science and Engineering of Carbon, Elsevier, 2016: pp. 125–152. https://doi.org/10.1016/B978-0-12-805256-3.00007-6.
[28] M. Smith, L. Scudiero, J. Espinal, J.-S. McEwen, M. Garcia-Perez, Improving the deconvolution and interpretation of XPS spectra from chars by ab initio calculations, Carbon N y. 110 (2016) 155–171, https://doi.org/10.1016/j.carbon.2016.09.012.
[29] T. Ishii, T. Kyotani, Temperature Programmed Desorption, in M. Inagaki, F. Kang (Eds.), Materials Science and Engineering of Carbon, Elsevier, 2016: pp. 287–305. https://doi.org/10.1016/B978-0-12-805256-3.00014-3.
[30] D. Han, Y. Liu, Y. Lv, W. Xiong, F. Hao, H. Luo, P. Liu, In situ oxygen-induced zigzag graphene as metal-free catalyst for hydrogen activation in nitroarenes hydrogenation, Carbon N y 203 (2023) 347–356, https://doi.org/10.1016/j.carbon.2022.11.071.
[31] M. Tamura, K. Shimizu, A. Satsuma, Comprehensive IR study on acid/base properties of metal oxides, Appl. Catal. A 433–434 (2012) 135–145, https://doi.org/10.1016/j.apcata.2012.05.008.